Magnetic Properties of Co Films on Cu/Si(110) and Cu(111)

G. Mankey – University of Alabama

et al.

Citation of published version:

Maat, S., et al. (2000): Magnetic Properties of Co Films on Cu/Si(110) and Cu(111). *Physical Review B*, 61(6). DOI: https://doi.org/10.1103/PhysRevB.61.4082

Magnetic properties of Co films on Cu/Si(110) and Cu(111)

S. Maat, M. T. Umlor,* D. Orgassa, H. S. Cho,† O. Koshkina,‡ H. Fujiwara, and G. J. Mankey
Department of Physics and Astronomy and Center for Materials for Information Technology, University of Alabama, Tuscaloosa, Alabama 35487

(Received 16 December 1998; revised manuscript received 23 July 1999)

The magnetic anisotropy of strained epitaxial Co films deposited on strained Cu(111) on Si(110) and miscut Cu(111) are reported. First, a Cu(111) buffer layer with an in-plane strain is formed by epitaxial growth on Si(110). Co films deposited on the buffer layer develop a uniaxial anisotropy axis originating from the strain along the twofold axis of the Si(110) surface. The magnetic anisotropy of this film is compared to that of a Co film deposited on a miscut Cu(111) single crystal with uniaxial step-induced anisotropy in the Co layer. The measured hysteresis loops are compared to hysteresis loops simulated within a Stoner-Wolfarth model with a varying fraction of uniaxial and triaxial anisotropies. The measurements and the model are in qualitative agreement and reveal uniaxial and triaxial anisotropies of the same order of magnitude for both systems.

I. INTRODUCTION

Multilayers of Co and Cu are frequently chosen materials for spin-valve elements in read heads for magnetic storage devices.[1] Epitaxial Co/Cu(111) multilayers exhibit a polarization of the Cu conduction band due to a good band matching between the Co and Cu, which is an essential feature for a high GMR ratio.[2] A reduced antiferromagnetic coupling between the Co layers is thought to originate from the fact that there are no extremal spanning vectors of the Fermi surface of Cu along the normal direction.[3] This feature is essential for a low coercivity free layer. Recently, it was reported that reduced antiferromagnetic coupling of Co layers through Cu(111) spacers can be attributed to stacking faults in the films and reduction of stacking faults resulted in complete antiferromagnetic coupling.[4] Since these films are deposited on Cu(111) substrates, it is not possible to determine their transport properties. Previous studies have shown that sputtered Cu(111) films on Si(110) exhibit good epitaxial growth.[5,6] The development of methods to produce and characterize such films on low conductivity substrates is essential for transport property measurements.

In this paper, we compare the magnetic behavior of Co grown on a strained Cu(111)/Si(110) buffer to that of a Co film grown on a miscut Cu(111) single crystal to determine differences in the magnetic properties of Co films grown on Cu buffer layers as opposed to Cu single crystals. The buffer layer should be smooth since the Néel ''orange peel'' coupling through conductive spacers increases the ferromagnetic coupling of the Co layers. It should provide a good fcc(111) oriented template for the subsequent Co layers. In addition, if a geometry with the current flowing parallel to the plane of the spin-valve is used, the buffer layer is required to be as thin as possible to minimize the amount of shunting.

We found that for a thin buffer layer, the interfacial strain at the Cu/Si interface is not completely relieved. This strain is transmitted through the buffer layer into the subsequent Co film, where it induces a uniaxial anisotropy. The combination of the uniaxial and triaxial crystalline anisotropy in the plane of the film gives a characteristic hysteresis loop shape similar to that observed for Co films deposited on a miscut Cu(111) single crystal substrate. The magnetic hysteresis as a function of azimuthal angle is compared to a model using the Stoner-Wolfarth formalism.

II. EXPERIMENTAL PROCEDURE

The Si(110) substrates were prepared by exposure to 255 nm ultraviolet radiation for 1 day followed by a 1 min dilute HF (10%) dip prior to insertion into the ultrahigh vacuum deposition chamber through a load lock. The substrates were transported from the HF etch into the load lock and pumped down to a pressure of 1.5×10^{-6} torr in about 10 min. Low-energy electron diffraction (LEED) confirmed that this procedure produces a well-ordered hydrogen-terminated single crystal surface.[7] The films were deposited at a growth pressure of 2×10^{-9} torr with the main component of the background gas being CO. Typical deposition rates were 10 pm/s for Cu and 1 pm/s for Co. Film thickness was determined using a quartz crystal microbalance located the same distance from the source as the substrate. The films were deposited with the substrate at room temperature.

Crystalline quality was monitored by reflection high-energy electron diffraction (RHEED) with an incident electron beam energy of 15 keV. Figure 1 shows RHEED data of a multilayer film deposited by vapor deposition on Si(110). The RHEED pattern shows that a Cu(111) buffer layer is formed on the Si(110) substrate and subsequent deposition of Co and Cu on this buffer exhibit similar orientations. The film is rough on the atomic scale since spots characteristic of transmission of electrons through island structures are observed. The roughness of the multilayer in Fig. 1 was measured *ex situ* with an atomic force microscope and found to have a root-mean-square roughness of 0.4 nm (2 atomic layers) with terrace sizes in the range of 20–30 nm. LEED I-V curves of the deposited films indicate that the stacking of the Co is fcc(111) as opposed to hcp(0001) for films on Cu/Si(110). The roughness affects the stacking, since Co growth on single crystal Cu(111) substrates exhibit LEED I-V curves, which have a portion of the film with hcp stacking. This is consistent with a previous study of room temperature growth of Co on Cu(111), which found a mixture of fcc and hcp phases.[8]

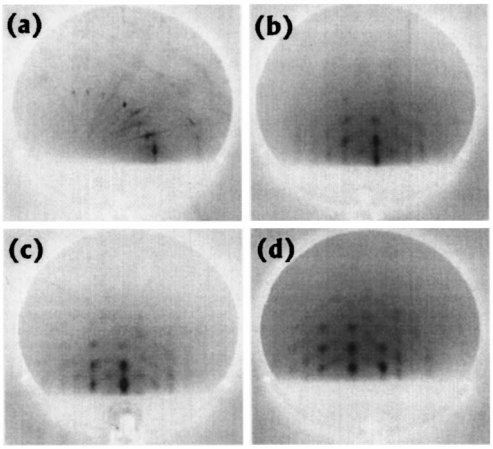

FIG. 1. RHEED of (a) Si(110), (b) 5 nm Cu/Si(110), (c) 3 nm Co/5 nm Cu/Si(110), and (d) 3 nm Cu/3 nm Co/5 nm Cu/Si(110). The incident electron energy was 15 keV for all measurements. The sixfold spots characteristic of a fcc(111) or hcp(0001) surface are observed in all the films.

III. STRAIN OF Cu/Si(110) FILMS

The stereographic projections that show the epitaxial relation between the major crystallographic directions of the Si(110) and the Cu(111) surfaces as verified by RHEED data, x-ray diffraction[5,6] and neutron-diffraction[9] measurements are shown in Fig. 2. The Cu[111] axis, which is perpendicular to the plane of the film will be denoted with z', while the Cu$[\bar{1}10]$ is denoted with y' and the Cu$[11\bar{2}]$ with x'. The Cu[100], [010], and [001] are denoted as x, y, and z, respectively. The epitaxial relation of Cu(111) on Si(110) with Cu$[\bar{1}10]\|$Si[001] shown in Fig. 3 illustrates that Cu films grown on this substrate incorporate a high amount of strain. The bulk lattice mismatch gives a 6% expansion of the Cu film along the Si[001] direction (Cu$[\bar{1}10]$ direction) and a 13% compression along the Si$[1\bar{1}0]$ (Cu$[11\bar{2}]$ direction).

The strain tensor in the $x'y'z'$ coordinate sysytem, which is assumed to be diagonal is

$$e_{i'j'}=\begin{bmatrix} 1-\delta & 0 & 0 \\ 0 & 1 & 0 \\ 0 & 0 & \rho(2-\delta) \end{bmatrix}, \tag{1}$$

where ρ is the Poisson ratio with $-\frac{1}{2}\leqslant\rho\leqslant 0$ and δ is the strain-relief parameter. $\delta=0$ means no strain relief. The following analysis will show how δ is related to the uniaxial anisotropy.

The elasticity tensor transforms into the coordinate system (x,y,z) like

$$e_{ij}=\sum_{k'l'}\gamma_{ik'}\gamma_{jl'}e_{k'l'}, \tag{2}$$

where $\gamma_{ik'}$ are the direction cosines between axis i in the (xyz) coordinate system and k' an axis in the $(x'y'z')$ system. For the case discussed here

$$e_{xx}=1/2e_{x'x'}+1/6e_{y'y'}+1/3e_{z'z'}, \tag{3a}$$

$$e_{yy}=1/2e_{x'x'}+1/6e_{y'y'}+1/3e_{z'z'}, \tag{3b}$$

$$e_{zz}=2/3e_{y'y'}+1/3e_{z'z}, \tag{3c}$$

$$e_{xy}=e_{yx}=-1/2e_{x'x'}+1/6e_{y'y'}+1/3e_{z'z'}, \tag{3d}$$

$$e_{xz}=e_{zx}=-1/3e_{y'y'}+1/3e_{z'z'}, \tag{3e}$$

$$e_{yz}=e_{zy}=-1/3e_{y'y'}+1/3e_{z'z'}, \tag{3f}$$

with $\rho=-\frac{1}{2}$, which corresponds to a high degree of elasticity.

The magnetoelastic energy f_σ is usually written as

$$\begin{aligned} f_\sigma=&B_1[e_{xx}\alpha_1^2+e_{yy}\alpha_2^2+e_{zz}\alpha_3^2]+B_2[e_{xy}\alpha_1\alpha_2+e_{xz}\alpha_1\alpha_3 \\ &+e_{yz}\alpha_2\alpha_3]=B_1[1/3e_{z'z'}+1/2e_{x'x'}+1/6e_{y'y'} \\ &+1/2(e_{y'y'}-e_{x'x'})\alpha_3^2]+B_2[1/2(e_{y'y'}-e_{x'x'})\alpha_1\alpha_2 \\ &-1/3e_{y'y'}(\alpha_1\alpha_2+\alpha_2\alpha_3+\alpha_1\alpha_3)+1/3e_{z'z'}(\alpha_1\alpha_2 \\ &+\alpha_2\alpha_3+\alpha_1\alpha_3)], \end{aligned} \tag{4}$$

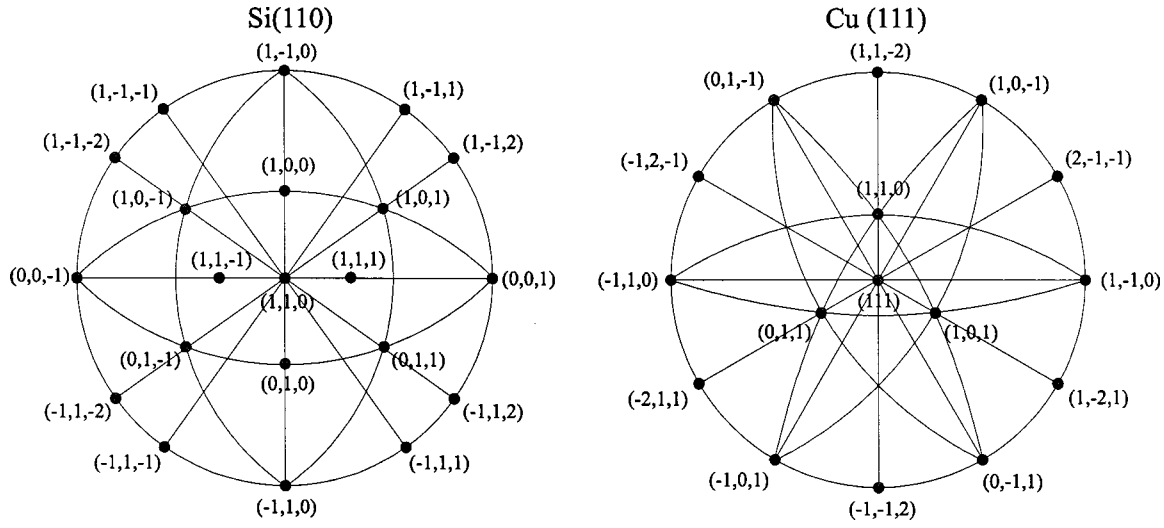

FIG. 2. Stereographic projection of the Si(110) surface and the Cu(111) surface.

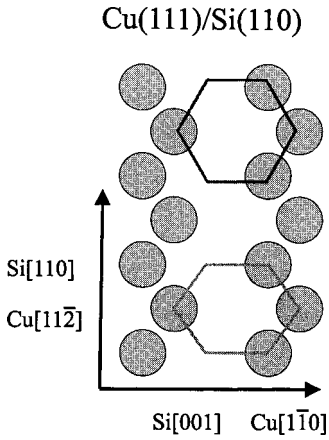

FIG. 3. Relationship of Cu(111) (illustrated as hexagons) lattice to the Si(110) lattice. At the top, the Cu hexagon is drawn unstrained, so the corners of the hexagon do not align with the Si atoms and the film is not epitaxial. The distorted hexagon at the bottom illustrates how large the in plane strain must be to have an epitaxial film.

where B_1 and B_2 are the magnetoelastic constants and the α_i are the direction cosines of the magnetization vector in the (xyz) coordinate system. These quantities are related to the polar and azimuthal angles Θ and φ of the Cu(111) crystal, with φ in the (111) plane and Θ the angle between $[111]$ and $[11\bar{2}]$ (z' and x') by

$$\alpha_1=\frac{1}{\sqrt{3}}[\sqrt{2}\cos(\varphi-120°)\sin\Theta+\cos\Theta], \tag{5a}$$

$$\alpha_2=\frac{1}{\sqrt{3}}[\sqrt{2}\cos(\varphi+120°)\sin\Theta+\cos\Theta], \tag{5b}$$

$$\alpha_3=\frac{1}{\sqrt{3}}[\sqrt{2}\cos\varphi\sin\Theta+\cos\Theta]. \tag{5c}$$

The expression

$$\alpha_1\alpha_2+\alpha_2\alpha_3+\alpha_1\alpha_3=-\tfrac{2}{3}\sin^2\Theta+\tfrac{7}{12}\sin^4\Theta \tag{6}$$

is only dependent on the polar angle and thus it gives no contribution to the in-plane anisotropy. For calculation of in-plane anisotropy, the polar angle is $\Theta=90°$ and the magnetoelastic anisotropy gives the uniaxial contribution

$$f_\sigma=\frac{(B_1+B_2)}{3}(e_{y'y'}-e_{x'x'})\cos^2\varphi=\frac{(B_1+B_2)}{3}\delta\cos^2\varphi, \tag{7}$$

which is a linear function of δ. The sign of δ determines whether $[1\bar{1}0]$ or $[11\bar{2}]$ is the easy axis. The measured easy axis is the $[1\bar{1}0]$ axis, which gives δ a negative sign, since $B_1=-2.9\times10^6$ and $B_2=-1.71\times10^6$ for Co[11].

IV. HYSTERESIS LOOP MEASUREMENTS

Longitudinal magneto-optic Kerr effect (MOKE) measurements of the in-plane component of magnetization for 3 nm Cu/3 nm Co/10 nm Cu/Si(110) film are shown in Fig. 4.

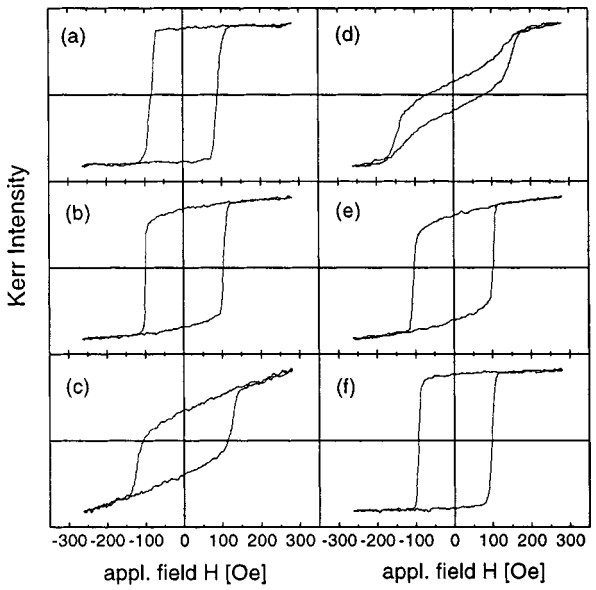

FIG. 4. Hysteresis loops of 3 nm Cu/3 nm Co/10 nm Cu/Si(110) measured with MOKE with the in-plane field applied at an angle Φ with respect to the [001] direction of the Si substrate (easy axis of magnetization). (a) $\Phi=0°$, (b) $\Phi=30°$, (c) $\Phi=60°$, (d) $\Phi=90°$, (e) $\Phi=120°$, (f) $\Phi=150°$. The unusual loop shape for the $[1\bar{1}0]$ direction of Si ($\Phi=90°$) is characteristic of a combination of uniaxial and triaxial anisotropy.

These measurements reveal an unusual loop shape for the field applied along the Si$[1\bar{1}0]$ direction [Fig. 3(d)], which is a loop characteristic of a magnetic hard axis of a film with a combination of uniaxial and triaxial in-plane anisotropy. It is most likely that uniaxial anisotropy in the Co has its origin in the uniaxial strain in the film produced by the contraction of the Co lattice along the $[1\bar{1}0]$ direction of the Si substrate. For thinner buffer layers such as the multilayer films shown in Fig. 1, the uniaxial anisotropy was so large that no triaxial component was observed. The triaxial component has its origin in the sixfold crystalline anisotropy, which is much weaker than that introduced by the high amount of uniaxial strain at the Cu/Si(110) interface. As the strain is relieved by the formation of misfit dislocations in thicker buffer layers, the triaxial anisotropy becomes comparable to the uniaxial anisotropy.

Longitudinal Kerr effect measurements of the in-plane component of magnetization for 3 nm Cu/3 nm Co/Cu(111) are shown in Fig. 5. The data shows the same qualitative behavior as the Co films grown on Cu/Si(110). In comparison with the Co film grown on Cu/Si(110), the Co film grown on Cu(111) exhibits a larger remanent magnetization along the hard axis. Since the (111) surface of a cubic crystal can exhibit only a surface triaxial anisotropy term, the uniaxial contribution must originate from another anisotropy in the film. The Cu(111) crystal is cut with a precision of 1°, which gives a single atomic step at most every 70 atoms. The miscut is the origin of the uniaxial anisotropy term. Magnetic surface anisotropy, induced by step edges on miscut single crystals, has been studied experimentally[11–19] and theoretically.[19,20] In the case of Co grown on miscut Cu(100) (Refs. 11–16) and Fe on Ag(100) (Ref. 17) step edges of the [110] type were found to add an uniaxial anisotropy to the

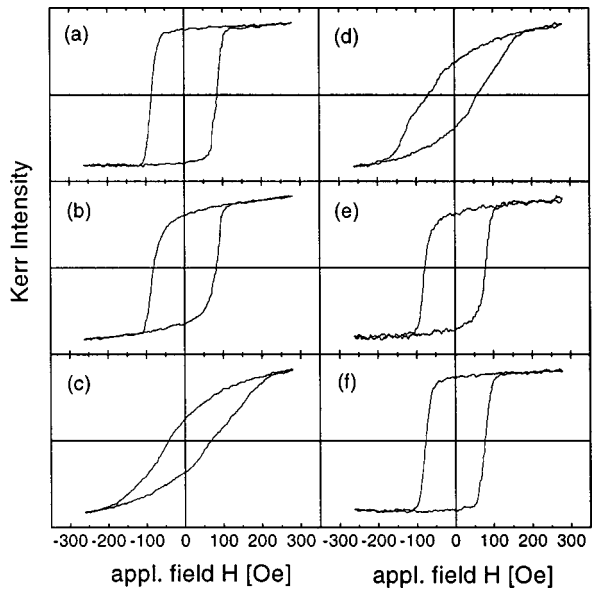

FIG. 5. Hysteresis loops of 3 nm Cu/3 nm Co/Cu(111) measured with MOKE with the in-plane field applied as a function of angle relative to the $[\bar{1}10]$ direction of Cu (easy axis of magnetization). (a) $\Phi=0°$, (b) $\Phi=30°$, (c) $\Phi=60°$, (d) $\Phi=90°$, (e) $\Phi=120°$, (f) $\Phi=150°$. The unusual loop shape for the $[\bar{1}01]$ Cu direction is characteristic of a combination of uniaxial and triaxial anisotropy.

surface crystalline biaxial anisotropy of the (100) facets. The overall easy axis was found to be parallel to the step edges in both systems. For the case of Fe on W(100) (Ref. 18) however, the easy axis was found to be perpendicular to the [110] type step edges. So the easy axis of Co on miscut Cu(111) may be either parallel or perpendicular to the step edges.

Co grows in a simultaneous multilayer mode at room temperature on Cu(111),[23] so the steps of a miscut substrate are reproduced in the ultrathin regime by the Co films. If the Co film grows in patches on the steps and the patches are strained differently in directions parallel and perpendicular to the step edges, a uniaxial magnetoelastic anisotropy is created. Using the bulk anisotropy constants of Co, a biaxial strain can produce an easy axis parallel or perpendicular to the step edges of Cu(100),[20] depending on the amount of strain-misfit perpendicular to the steps. Thus the origin of the uniaxial anisotropy of both Co grown on Cu/Si(110) and Co on Cu(111) can be related to strain.

V. HYSTERESIS LOOP MODELING

The films show an in-plane easy axis in contrast to films grown in the monolayer thickness regime. In addition, magnetic force microscopy measurements of the films in remanence showed no clear domain structures for the fresh films that were studied with MOKE. After a few days in air, the film began to oxidize around the edges and domain structures characteristic of a perpendicular magnetization component began to emerge. Ultrathin films exhibit an out-of-plane easy axis, which originates from the larger proportion of surface anisotropy.[10] The perpendicular anisotropy is weak even in monolayer-thick films, so the contribution of the surface anisotropy can be neglected in films 3 nm thick (15 layers). The observed hard axis hysteresis loop can be modeled by a

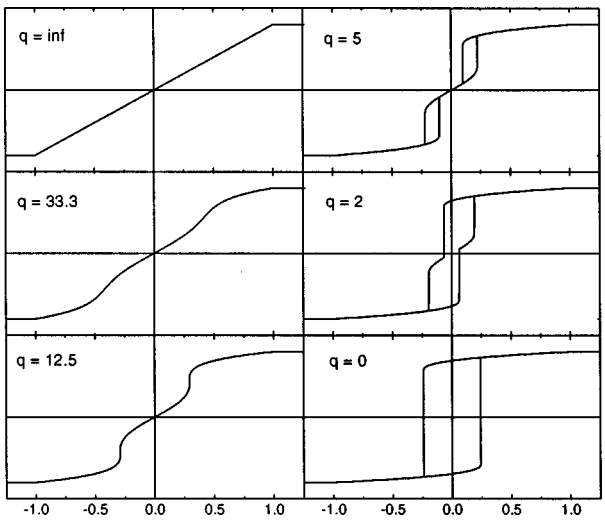

FIG. 6. Calculated hard axis ($\theta=90°$) hysteresis loops for uniaxial and triaxial anisotropy assuming coherent domain rotation of the magnetization with different uniaxial to triaxial ratios $q=K_u/K_t$. (a) $q=\infty$, pure uniaxial anisotropy, (b) $q=33.3$, (c) $q=12.5$, (d) $q=5$, (e) $q=2$, (f) $q=0$, pure triaxial anisotropy.

Stoner-Wolfarth formalism describing coherent rotation of magnetic domains using an energy density term including uniaxial and triaxial anisotropies,[20–22]

$$E=-M_sH\cos\phi+K_u\sin^2(\theta-\phi)+K_t\sin^2 3(\theta+\beta-\phi),$$

where M_s is the saturation magnetization, ϕ is the angle between the applied field, H, and the magnetization, and θ is the angle of the applied field relative to the uniaxial easy axis with anisotropy constant K_u, and β is the angle between uniaxial easy axis and one crystalline triaxial easy axis with anisotropy constant K_t. Minimization of the energy with respect to the angle of magnetization gives a critical field of

$$H_k=\frac{2}{M_s}(K_u+9K_t).$$

Normalizing by $2(K_u+9K_t)$ the expression for the energy density, f, can be written as

$$f=-h\cos\phi-\frac{q}{4(q+9)}\cos 2(\theta-\phi)$$

$$-\frac{1}{4(q+9)}\cos 6(\theta+\beta-\phi);$$

here $q=K_u/K_t$, the ratio of uniaxial to triaxial anisotropy and $h=H/H_k$ is the normalized field.

Figure 6 shows the calculated results of the component of magnetization along the hard axis with the applied field along the hard axis. The parameter q is the relative amount of uniaxial anisotropy when the uniaxial easy axis is parallel to the crystalline easy axes ($\beta=0^0$). The model shows that for q close to 12.5 the steps occurring in the modeled loops resemble the shape of the measured hard axis loop in Fig. 4(d). In contrast to the measurement the simulation shows no remanence, since the model accounts only for a single domain state. A remanence for a single domain can arise by a

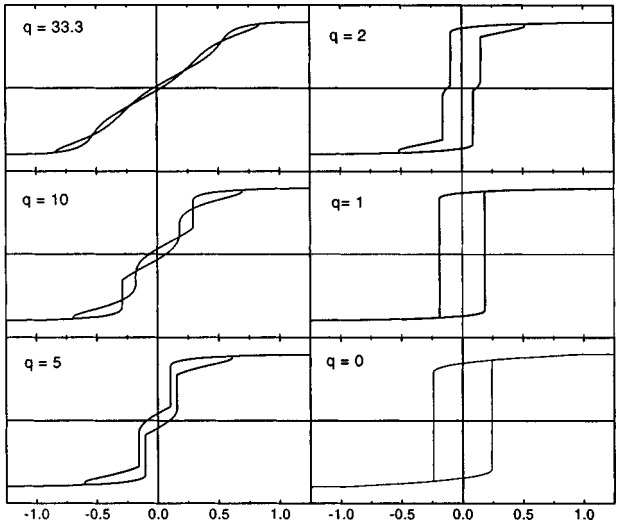

FIG. 7. Calculated hard axis ($\theta=90°$) hysteresis loops for misaligned ($\beta=10°$) uniaxial and triaxial anisotropy assuming coherent domain rotation of the magnetization vector with different uniaxial to triaxial ratios $q=K_u/K_t$. (a) $q=33.3$, (b) $q=10$, (c) $q=5$, (d) $q=2$, (e) $q=1$, (f) $q=0$, pure triaxial anisotropy.

misalignment of the uniaxial easy axis from the crystalline triaxial easy axis. Figure 7 shows the calculated results for the hard axis magnetization when the angle between the uniaxial easy axis and the crystalline triaxial easy axis is $\beta=10^0$. The loop calculated for $q=5$ shows a remanent magnetization though it exhibits sharper switching of magnetization than the measured loop shown in Fig. 4(d). Both remanence and smoothening of the magnetic switching can be achieved, if an angular distribution of uniaxial anisotropy is assumed. The result of a calculation for a Gaussian distribution in β with halfwidth $\beta=10^0$ for $q=5$ is shown in Fig. 8.

Distribution of magnetization in the Co layers due to distribution of the local anisotropy and noncoherent rotation of magnetization reversal process along the hard axis are also sources of smoothening of magnetization curves. The calculated results also show increasing remanence along the hard axis with a decreasing ratio of crystalline triaxial anisotropy to uniaxial anisotropy. The remanent magnetization of the Cu/Co/Cu(111) for the hard axis [Fig. 4(d)] is larger than

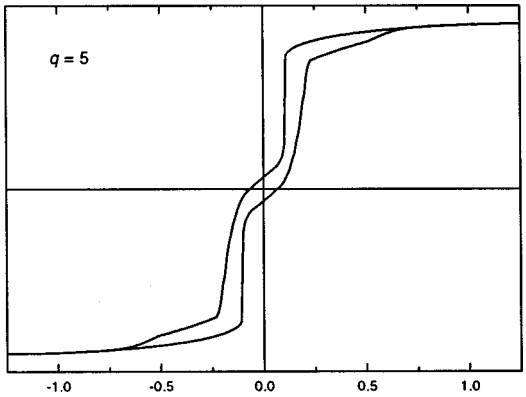

FIG. 8. Calculated hard axis ($\theta=90°$) hysteresis loops for an angular distribution in β for $q=2$. The assumed half width for β is 10°.

that of the Cu/Co/Cu/Si(110) [Fig. 3(d)], implying that the Co layer on the single crystal Co(111) has a relatively larger crystalline anisotropy than the Co layer on Cu/Si(110). The larger crystalline anisotropy appears to be due to better crystallinity of the Co layer on single crystal Cu(111), as evidenced by the RHEED measurements.

VI. SUMMARY

An unusual uniaxial anisotropy was observed in Co films both on Cu(111)/Si(110) and a Cu(111) single crystal, where the uniaxial anisotropies are related to uniaxial strain in the former case and a slight miscut of the Cu(111) in the latter case. The measured hysteresis loops were modeled within a Stoner-Wolfarth formalism incorporating uniaxial and triaxial anisotropies. The origin of the uniaxial anisotropy term originates from the uniaxial stress present in the epitaxial relationship of Cu(111) on Si(110) and the step anisotropy for miscut Cu(111) substrate.

ACKNOWLEDGMENTS

The authors would like to thank H. Jiang and W. D. Doyle for helpful discussion on M-H loop modeling. This research was supported by DOD under Grant Nos. DAAH04-94-6-0251 and DAAH04-96-1-0316 and by NSF under Grant No. DMR-9809423.

*Present address: Department of Physics and Astronomy, University of Wisconsin–Oshkosh, Oshkosh, WI 54901.
†Present address: Seagate Technologies, Minneapolis, MN 55401.
‡Present address: Seagate Technologies, Boulder, CO 80301.

[1] J. C. S. Kools, IEEE Trans. Magn. **32**, 3165 (1996).
[2] P. Bruno and C. Chappert, Phys. Rev. Lett. **67**, 1602 (1991).
[3] M. D. Stiles, Phys. Rev. B **48**, 7238 (1993).
[4] M. Zheng, J. Shen, Ch. Mohan, P. Ohresser, J. Barthel, and J. Kirshner, Appl. Phys. Lett. **74**, 425 (1999).
[5] H. Jiang, T. J. Klemmer, J. A. Barnard, W. D. Doyle, and E. A. Payzant, Thin Solid Films **315**, 13 (1998).
[6] H. Jiang, T. J. Klemmer, J. A. Barnard, E. A. Payzant, J. Vac. Sci. Technol. A **16**, 3376 (1998).
[7] B. G. Demczyk, R. Naik, G. Auner, C. Kota, and U. Rao, J. Appl. Phys. **75**, 1956 (1994).
[8] M. T. Kief and W. F. Egelhoff, Jr., Phys. Rev. B **47**, 10 785 (1993).
[9] S. Maat, L. Shen, G. J. Mankey, J. L. Robertson, M. L. Crow, T. C. Schulthess, and W. H. Butler (unpublished).
[10] F. Huang, G. J. Mankey, and R. F. Willis, J. Appl. Phys. **75**, 6406 (1994).
[11] H. P. Oepen, C. M. Schneider, D. S. Chuang, C. A. Ballentine, and R. C. O'Handley, J. Appl. Phys. **73**, 6186 (1993).
[12] W. Wulfhekel, S. Knappmann, and H. P. Oepen, J. Appl. Phys. **79**, 988 (1996).
[13] W. Weber, C. H. Back, A. Bischof, Ch. Würsch, and R. Allenspach, Phys. Rev. Lett. **76**, 1940 (1996).
[14] A. Berger, U. Linke, and H. P. Oepen, Phys. Rev. Lett. **6**, 839 (1992).
[15] S. T. Coyle and M. R. Scheinfein, J. Appl. Phys. **83**, 7040 (1998).
[16] H. A. Dürr, G. van der Laan, J. Vogel, G. Panaccione, N. B. Brooks, E. Dudzik, and R. McRath, Phys. Rev. B **58**, R11 853 (1998).

[17] R. K. Kawakami, E. J. Escorcia-Aparicio, and Z. Q. Qiu, Phys. Rev. Lett. **77**, 2570 (1996).
[18] J. Chen, and J. L. Erskine, Phys. Rev. Lett. **68**, 1212 (1992).
[19] M. Albrecht, T. Furubayashi, M. Przybylski, J. Korecki, and U. Gradmann, J. Magn. Magn. Mater. **113**, 207 (1992).
[20] D. S. Chuang, C. A. Ballentine, and R. C. O'Handley, Phys. Rev. B **49**, 15 084 (1994).
[21] E. C. Stoner, and E. P. Wohlfarth, Philos. Trans. R. Soc. London, Ser. A **240**, 599 (1948).
[22] A. Thiaville, J. Magn. Magn. Mater. **182**, 5 (1998).
[23] F. Huang, M. T. Kief, G. J. Mankey, and R. F. Willis, Phys. Rev. B **49**, 3962 (1994).